

Optimal Design of a PZT Bimorph Actuator for Minimally Invasive Surgery

David J. Cappelleri, Graduate Research Assistant
Mary I. Frecker, Assistant Professor
Timothy W. Simpson, Assistant Professor

Pennsylvania State University
Department of Mechanical and Nuclear Engineering
University Park, PA 16802

ABSTRACT

A metamodel-based approach is developed to optimize the force and displacement performance of a piezoceramic bimorph actuator. A segmented design with a variable piezoceramic layer thickness is proposed, where the thicknesses of discrete piezoceramic segments are used as the design variables. Design of experiments and metamodeling techniques are employed to construct computationally inexpensive approximations of finite element simulations of the PZT bimorph actuator. The metamodels are then used in lieu of the actual FEM for optimization. Design objectives include maximum tip deflection, maximum grasping force, and maximum work available at the tip. The metamodels are also used to rapidly generate the design space and identify the Pareto frontier for the competing design objectives of maximum deflection and maximum force. The accuracy and efficacy of two types of metamodels—response surfaces and kriging models—are compared in this study. By optimizing the thickness of the piezoceramic layers, and by allowing the voltage applied to each segment to vary, dramatic improvements in deflection and force are obtained when compared to a standard straight bimorph actuator. The motivation for this design is the need in the field of minimally invasive surgery for improved grasping tools, where a pair of optimized bimorph actuators can be used as a simple grasping device.

Keywords: Piezoelectric Bimorph, Minimally Invasive Surgery, Sizing Optimization, Metamodeling

1. INTRODUCTION

A piezoelectric bimorph actuator is created by laminating layers of piezoelectric ceramic material (PZT) onto a thin sandwich beam or plate. When opposing voltages are applied to the two ceramic layers, a bending moment is induced in the beam (Figure 1)¹. A pair of cantilevered piezoelectric bimorph actuators can be used as a simple grasping device, where the bimorph actuators are used as active “fingers” as shown in Figure 2. Chonan, et al.² and Seki³ have designed PZT bimorph graspers for use in MEMS and robotics. Bar-Cohen, et al.⁴ and Lumia and Shahinpoor⁵ have designed bimorph actuator grippers using piezoelectric polymers.

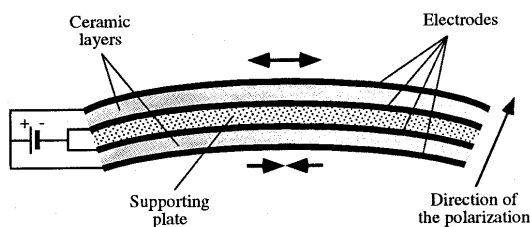


Figure 1. PZT Bimorph.

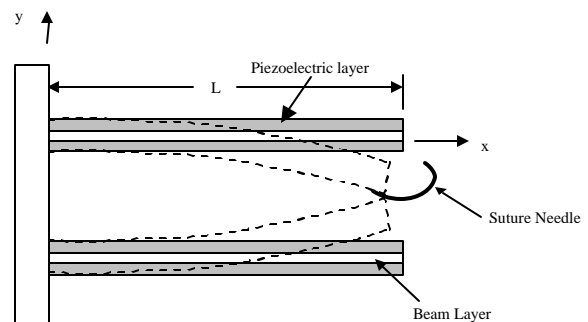


Figure 2. Bimorph Grasper.

The focus in this research is on the design of a PZT bimorph grasper for application to minimally invasive surgical (MIS) procedures. During MIS, small surgical tools and viewing equipment are introduced into a body cavity through long slender tubes. MIS requires several 3 to 10 millimeter incisions rather than a single large incision as in open surgery and offers the

benefits of reduced tissue trauma and improved patient recovery time^{6,7}. Today laparoscopic MIS is commonly used in abdominal procedures such as gall bladder removal; however, current tools used in MIS suffer from technical limitations in dexterity, control, and versatility^{6,8-11}. As a way to address the need for improved dexterity and control in MIS, we propose the use of an active end-effector such as the PZT bimorph grasper shown in Figure 2, which offers certain advantages over current MIS grasping tools. For instance, current laparoscopic end-effectors are mechanically actuated by long tendon wires or push rods which can be difficult to control precisely. The end-effector of a typical laparoscopic grasping instrument, as pictured in Figure 3, is used to grasp suture needles or tissue. By incorporating a simple controller with an active end-effector, the position input of the surgeon at the actuation handle can be converted to a voltage input to the active end-effector. Since the actuator material is integrated in the bimorph design directly into the working jaws of the end-effector, the surgeon can very precisely control the position of the grasper. Furthermore, a PZT bimorph grasper has no hinges or pin joints, allowing for easy sterilization when compared to pin-jointed designs.



Figure 3. Laparoscopic Grasper.

Several researchers have explored innovative designs for MIS tools to address the need for improved dexterity, control, and sensing. Melzer¹⁰ does an extensive review of advanced concepts for “intelligent” endoscopic instruments, including a grasping instrument with hingeless jaws where shape memory alloy materials are used to close the jaws. To provide both improved dexterity and tactile sensing, hand-like end-effectors have been developed by Cohn, et al.⁸ and Sastry, et al.¹¹. Although these devices have displayed acceptable dexterity, they contain numerous millimeter-scale components and actuators and are limited in their force output capability. Other innovative surgical tools have been developed such as an elastic jaws grasping forceps which utilizes two elastic beams in place of a mechanical hinge joint¹². An active laparoscopic tool has been developed by Nakamura et al.¹³ using shape memory alloys which can bend to change its shape from straight to a circular arc. Finally, a piezoceramic inchworm actuator and compliant suture needle grasper has been designed by Canfield, et al.¹⁴ for laparoscopic surgery applications.

For MIS applications the critical design parameters of the surgical tools are the dimensions of the end-effector since it must be inserted into a 10.0 mm diameter (or smaller) tube. The performance of the grasper is also critical since it must be able to close completely from a 3.0 mm opening at the jaws while exerting a suitable force at the tip. The design requirements for this application are summarized in Table 1. It is estimated that 0.5 N is required to secure a 0.5 mm diameter suture needle in the jaws of the grasper while less force is required for grasping tissue.

Table 1. Design Requirements.

Geometry	3.0 mm opening at jaws; jaws able to close completely; jaws parallel when closed on 0.5 mm needle
Maximum Size	minimize length, 3.5 mm width, 9.5 mm thickness
Grasping Force	0.5 N at 0.5 mm jaw opening
Speed	≤200 ms gripper opening/closing time

For this analysis, the performance of the PZT bimorph actuator is evaluated in terms of the tip force and deflection. These performance criteria are determined by the thickness and width of the PZT layers, the length of the actuator, the material properties, and the applied voltage. A simple model of a standard bimorph actuator with constant layer thicknesses is used to determine its feasibility for the MIS grasper application; Equations 1 and 2 describe the tip deflection (d) and blocked force (F), respectively. Note that these equations do not take into account the sandwich beam layer and assume perfect bonding between the piezoceramic layers. The active material is assumed to be PZT5H with dielectric constant $\epsilon_{31} = -274.0 \text{ E}12 \text{ m/V}$ and elasticity constant $Y_{11} = 7.1 \text{ E}10 \text{ N/m}^2$. The applied voltage (V) is 100.0 V, the actuator length (L) is 5.4 cm, the total thickness (t) is 4.5 mm, and the width (W) is 3.0 mm. The force available at the tip is modeled as the blocked force (force exerted with no deflection), and the deflection is modeled as the free deflection. Both of these terms represent maximum values. The results from this preliminary analysis demonstrate that a standard straight bimorph with the specified design parameters is infeasible for the MIS application since there is insufficient grasping force and tip deflection.

$$d = \frac{4L^2 V d_{31}}{t^2} = 0.016 \text{ mm} \quad (1)$$

$$F = \frac{3}{4} d_{31} V \left(\frac{tW}{L} \right) Y_{11} = 0.365 \text{ N} \quad (2)$$

2. DESIGN APPROACH AND MODEL FORMULATION

To improve the deflection and force performance of the PZT bimorph actuator, a variable thickness design is proposed where the thickness of the piezoceramic layers is varied along the length. Since the analysis of the standard straight bimorph demonstrated that improvements are needed in both the tip deflection and force in order to meet the design requirements listed in Table 1, an optimization problem is formulated to simultaneously maximize the tip deflection and the available tip force for a given length bimorph actuator. A large tip deflection is required so that the jaws of the grasper can close completely, and a large tip force is required to securely grasp a suture needle and prevent it from rolling in the jaws.

The bimorph actuator is modeled as composite beam with a thin steel sandwich layer and PZT5H top and bottom layers. Rather than allowing the thickness of the PZT layers to vary continuously along the length, the layers are discretized into five sections to allow for simple modeling, where the thickness of each section, t_i ($i=1, \dots, 5$), are the design variables. A finite element model of the composite variable thickness design is created with standard cantilever supports at the base nodes; a representative figure of the model is shown in Figure 4. The finite element model consists of 1458 eight-node three-dimensional (brick) elements as shown in Figure 5. Each PZT section has three elements across its height and width, and 10 elements along the length. As the thickness of the PZT sections is varied in the optimization procedure, the number of elements remains constant. Node compatibility at the section boundaries is ensured through the use of transition elements as shown in Figure 4. These elements are formed by joining the end nodes from one piezoelectric section to the start nodes of the next piezoelectric section. The length of the transition elements, x_{tr} , remains constant. The steel beam is modeled using 486 brick elements, with each section having three elements along its height and width and 10 across the length. A summary of material properties is given in the Appendix.

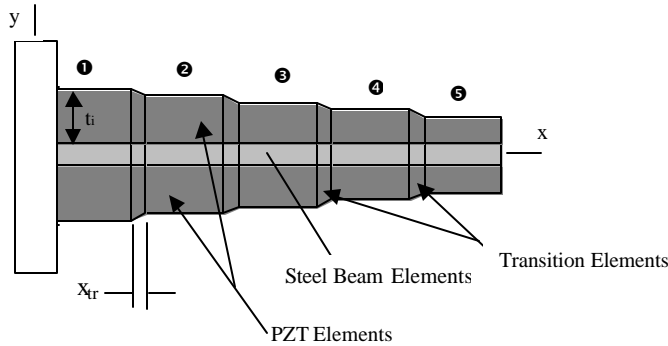


Figure 4. Variable Thickness Bimorph Actuator

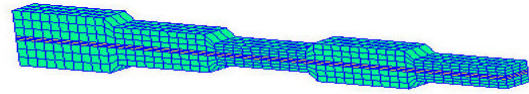


Figure 5. Finite Element Model of Variable Thickness Bimorph Actuator.

The finite element analysis is performed using ABAQUS, a commercial finite element software package¹⁵. Two types of FE analysis are conducted: one that predicts the free deflection of the bimorph and one that predicts the blocked force while subjecting the actuator to a prescribed input voltage. Since the operating frequency is low (on the order of 1-2 Hz) in MIS applications, only a quasi-static response is considered. The blocked force condition is simulated by constraining the nodes at the tip of the bimorph in the y-direction. To simulate applying voltage to the PZT layers, a linear perturbation step is used in ABAQUS. The initial state or base state of the model is unloaded, i.e., no voltage is applied to any of the nodes of the PZT elements. Loading is applied during the perturbation step and is defined as the change in state from the base state. During the perturbation step, positive voltage is applied to the outer nodes of the PZT elements, i.e., to those farthest away from the steel sandwich layer. Negative voltage is applied to the nodes that are shared between the steel and PZT elements to induce a potential difference across the PZT layers. The free deflection response is the y-direction deflection of the tip nodes,

while the blocked force response is the vector sum of the vertical reaction forces at the constrained tip nodes. The geometry parameters for the model are summarized in the Appendix. The results of the ABAQUS FEA have been verified using a known analytical model¹⁶ for a standard bimorph deflection with uniform thickness. The error in the ABAQUS model increases as the uniformly thick PZT layer approaches its lower bound, and decreases as it moves towards the upper bound. The average percentage error between the two models throughout the entire design space is 9.0%.

Much of the related work in the area of design and analysis of bimorph actuators is focused on vibration control and transducer applications¹⁷⁻²⁰. Modeling, design, and optimization of piezoelectric bimorphs and structures have been considered by several researchers, but these methods primarily use constant thickness piezoelectric layers or elements. For example, Crawley and de Luis²¹, Cunningham, et al.²², Franco-Correia, et al.²³, and Low and Guo²⁴ model bimorph actuators with constant PZT and substrate layer thicknesses. Crawley and de Luis²¹ and Crawley and Anderson²⁵ have developed analysis models of beams with individual piezoelectric elements bonded to the surface of the substrate and with them embedded in a laminate composite beam. In both instances the thickness of the piezoelectric layers remained constant within or on the beam. Low and Guo²¹ develop a model of a three-layer piezoelectric bimorph beam incorporating hysteresis effects. The bimorph is simply supported with an externally supplied force applied and the mid-point deflection is predicted. The piezoelectric layers thicknesses are held constant and the deflection at the mid-point is determined using the total energy stored in the beam due to the applied electric field, external force, and coupling of both the applied electric field and external force. Cunningham, et al.²² explores the relationship between the thickness of a piezoelectric actuator and the thickness of the cantilever that it is mounted to. This is done by observing the effective bending moment induced in the beam, which for a given piezoelectric layer and cantilever thickness is only a function of the Young's modulus of the cantilever. Thus, for each material there is an optimum thickness for maximum actuation because a thicker actuator produces larger actuation until the stiffening effect of the actuator dominates. However, this model is used only on actuators with constant thickness and fails when the cantilever thickness is not sufficiently thin, Franco-Correia et al.²³ optimizes the constant thickness piezoelectric layers surface bonded to a substrate for the best deflection characteristics. Thickness optimization of piezoceramic transducers is done by Wolf et al.²⁶. Here the piezoceramic layer is bonded to the stator of an ultrasonic traveling wave motor and the thickness is optimized for maximal energy transfer, i.e., maximum electromechanical coupling. Relatively thick piezoceramic layers produce the best results for this application. Topology optimization methods have also been devised to optimize various properties of piezoelectric composite structures²⁷. The work in this paper presents a novel method for modeling and optimization of a PZT bimorph actuator with variable PZT layer thicknesses surface mounted continuously on the top and bottom of a substrate. Here the substrate thickness is held constant while variations in the applied electric field across each piezoceramic are allowed.

3. SOLUTION APPROACH

To facilitate optimization of the section thicknesses of the PZT bimorph actuator, a metamodel-based approach is proposed. Metamodeling involves the use of design of experiments to sample the design space defined by the bounds on the design variables ($1 \text{ mm} \leq t_i \leq 3 \text{ mm}$, $i = 1, \dots, 5$). Data is generated to construct inexpensive-to-run approximations of the ABAQUS finite element analysis. The approximations are then used in lieu of the FEA simulation, facilitating exploration of the design space and design optimization. A flowchart illustrating the implementation of our approach is shown in Figure 5.

As seen in Figure 6, after identifying the lower bounds (l.b.) and upper bounds (u.b.) for the design variables, the next step is to select an appropriate experimental design to sample the design space. A face-centered central composite (CCF) design²⁸ is used to sample each design variable at one of three possible levels: 1.0 mm, 2.0 mm, and 3.0 mm. Posing the problem in terms of optimal discrete section thicknesses rather than a continuously varying shape allows for solutions that are easily fabricated from commercially available PZT ceramic layers. With five section thicknesses each with three potential levels, a total of $3^5 = 243$ possible design combinations exist; however, we can sample the design space using 27 points based on the CCF design to generate a sufficient amount of data to fit a full second-order response surface model to approximate the FEA results. At each of these 27 points, the free deflection and blocked force of the PZT bimorph actuator is computed, and two different types of metamodels—response surfaces and kriging models—are employed to construct approximations of the resulting data. Response surfaces are described briefly in the next section; an overview of kriging follows in Section 3.2.

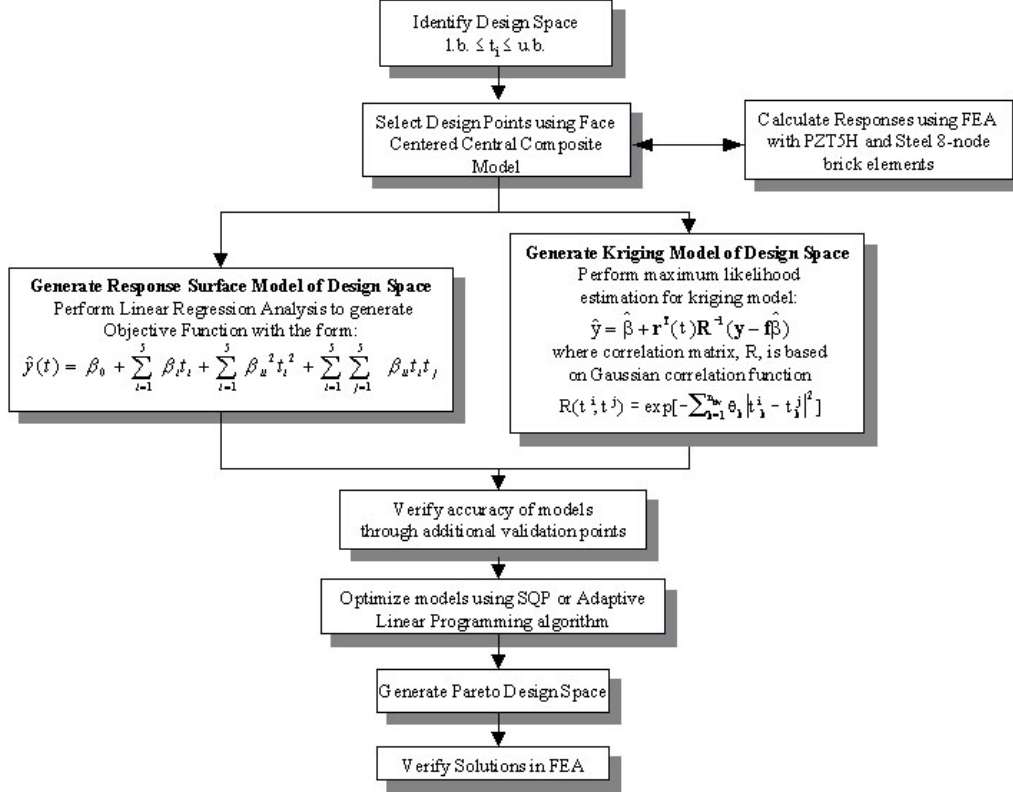


Figure 6. Solution Approach.

3.1. Response Surface Models

As shown in the left branch of Figure 6, the data from ABAQUS is used to construct full second-order response surface models of free deflection and blocked force using least squares regression. The general form of the second-order response surface model is shown in Equation 3, where $\hat{y}(t)$ is the predicted response, t_i are the design variables, and b_{ij} are the coefficients used to fit the model and are obtained from the least squares regression. A complete description of response surface models and least squares regression can be found in, e.g., Myers and Montgomery²⁹.

$$\hat{y}(t) = b_0 + \sum_{i=1}^5 b_i t_i + \sum_{i=1}^5 b_{ii} t_i^2 + \sum_{i=1}^5 \sum_{j=1}^5 b_{ij} t_i t_j \quad (3)$$

Equation 3 is fit to the free deflection and blocked force data that is generated from ABAQUS using the CCF design. Since the responses are modeled as second-order polynomial functions of the design variables, optimization techniques such as mathematical programming can be easily applied to determine an optimum thickness configuration. A MATLAB³⁰ program utilizing a sequential quadratic programming (SQP) routine is used to determine the optimum PZT layer thickness values for the individual design objectives of maximum deflection and maximum force. The constraints on the design variables are the upper and lower bounds of the thickness parameters, 3.0 and 1.0 mm, respectively. Because mathematical programming methods such as SQP tend to converge quickly to a local optimum, a batch of 243 different feasible starting points is used in order to reasonably ensure that the global maximum is obtained.

Response surfaces are typically second-order polynomial models; therefore, they have limited capability to model accurately non-linear functions of arbitrary shape. Obviously, higher-order response surfaces can be used to model a highly non-linear design space; however, instabilities may arise³¹, and it is often difficult to generate sufficient sample data to estimate all of the coefficients in the polynomial equation, particularly in high dimensions. Hence, many researchers advocate the use of a *sequential* response surface modeling approach using move limits³² or trust region approaches³³.

Many sequential approximation approaches, however, are being developed for *single objective* optimization applications. Since much of engineering design is *multiobjective* in nature, it is often difficult to isolate a small region of good design which can be accurately represented by a low-order polynomial response surface model. Koch, et al.³⁴ discuss the difficulties encountered when screening large variable problems with multiple objectives as part of the response surface approach. Barton³¹ states that the response region of interest will never be reduced to a “small neighborhood” which is good for all objectives during multiobjective optimization. Therefore, there exists a need to investigate alternative metamodels with sufficient flexibility to build accurate *global approximations* of the design space; kriging is one such alternative, and it is described in the next section.

3.2. Kriging Model

Originally developed for spatial statistics and geostatistics, kriging is an interpolative approximation model that makes predictions based on an exponentially weighted sum of the known sample data. Kriging models are very flexible due to the wide range of correlation functions that can be chosen for building the model. Depending on the type of correlation function used, a kriging model can either “honor the data,” providing an exact interpolation of the data, or “smooth the data” in the presence of numerical noise³⁵. As discussed in Simpson, et al.³⁶, kriging models may be better suited for building approximations of deterministic computer experiments since they interpolate the data and are not restricted by assumptions on the nature of the random error in the observations which does not exist in deterministic computer simulations such as this FEA.

Kriging postulates a combination of a global model and departures of the following form:

$$y(\mathbf{t}) = f(\mathbf{t}) + Z(\mathbf{t}) \quad (4)$$

where $y(\mathbf{t})$ is the unknown function of interest, $f(\mathbf{t})$ is a known function of \mathbf{t} , and $Z(\mathbf{t})$ is the realization of a stochastic process with mean zero, variance σ^2 , and non-zero covariance. The $f(\mathbf{t})$ term in Equation (4) is similar to the polynomial model in a response surface, providing a “global” model of the design space. In many cases $f(\mathbf{t})$ is simply taken to be a constant term β where β is estimated from the n_s sample points³⁷; $f(\mathbf{t})$ is taken as a constant in this work. While $f(\mathbf{t})$ “globally” approximates the design space, $Z(\mathbf{t})$ creates “localized” deviations so that the kriging model interpolates the n_s sampled data points.

Predicted values using a kriging model are obtained using Equation 5:

$$\hat{y}(\mathbf{t}) = \beta + \mathbf{r}^T(\mathbf{t})\mathbf{R}^{-1}(\mathbf{y}-\mathbf{f}\beta) \quad (5)$$

where \mathbf{y} is a column vector which contains the sample values of a particular response (i.e., deflection or blocked force), \mathbf{f} is column vector of length n_s which is filled with ones when $f(\mathbf{t})$ in Equation 4 is taken as a constant, and \mathbf{r}^T is a correlation vector of length n between an unknown x and the sample data points. The correlation matrix, \mathbf{R} , in Equation 5 is defined in Equation 6, where n_{dv} = number of design variables, θ_k are the unknown correlation parameters used to fit the model, and t_k^i and t_k^j are the k^{th} components of the sample points t^i and t^j .

$$\mathbf{R}(t^i, t^j) = \exp \left[- \sum_{k=1}^{n_{dv}} \theta_k \left| t_k^i - t_k^j \right|^2 \right] \quad (6)$$

A kriging model is fit to the sample data using an iterative optimization procedure to determine the maximum likelihood estimates of the θ_k parameters that are used to fit the model; details of this optimization procedure can be found in Sacks, et al.³⁷ and Simpson, et al.³⁸. The simulated annealing algorithm from Goffe, et al.³⁹ is employed in this work to fit the kriging models for blocked force and deflection.

With response surface models, R^2 (the ratio of the model sum of squares to the total sum of squares) can be used to assess model accuracy²⁹. Since kriging models typically interpolate the sample data leaving no residuals, alternative validation measures must be used to assess model accuracy. Additional data points can be used to check the validity of a kriging model

by computing relevant error measures using Equations 7, 8 and 9. The maximum absolute error, average absolute error, and root mean square error (RMSE) can be computed from additional validation data as follows.

$$\text{max. abs. error} = \max. \{ |y_i - \hat{y}_i| \}_{i=1, \dots, n_{\text{error}}} \quad (7)$$

$$\text{avg. abs. error} = \frac{1}{n_{\text{error}}} \sum_{i=1}^{n_{\text{error}}} |y_i - \hat{y}_i| \quad (8)$$

$$\text{RMSE} = \sqrt{\frac{\sum_{i=1}^{n_{\text{error}}} (y_i - \hat{y}_i)^2}{n_{\text{error}}}} \quad (9)$$

In Equations 7-9, y_i is the true response value, \hat{y}_i is the predicted value from the kriging or response surface model, and n_{error} is the number of additional points used to assess the error. Once the model has been fit, validated, and deemed sufficiently accurate, it can be used for optimization. In this work, the Adaptive Linear Programming algorithm⁴⁰ is utilized to optimize the kriging models for free deflection and blocked force.

4. METAMODEL VALIDATION

For the response surface models, the minimum R^2 value is 0.9694, indicating a good fit since 97% of the variance in the data is explained by the response surface. In order to obtain a direct comparison of the accuracy of the two models, a set of random validation points is generated from ABAQUS using a 25-point random Latin Hypercube⁴¹. The free deflection and blocked force responses predicted by both models are compared to the actual values as determined by the FEM in ABAQUS. The maximum, average, and root mean squared errors, Equations 7-9, are summarized in Table 2. The error in the deflection responses are comparable for both models, with the response surface model having slightly lower maximum and average percent error. However, in the case of the blocked force response, the kriging model fits the data much more accurately. Based on the RMSE for both the deflection and blocked force response, the kriging model is more accurate than the response surface model.

Table 2. Metamodel Validation.

	RSM		Kriging Model	
	Deflection	Blocked Force	Deflection	Blocked Force
Maximum % Error	13.78	18.99	18.06	8.02
Average % Error	6.23	4.33	7.09	2.83
RMSE	1.08E-03	1.47E-02	1.20E-06	8.35E-05

5. OPTIMIZATION RESULTS

The FEA simulations are conducted using two sets of electrical inputs to the piezoceramic layers. The first set of simulations is conducted using a constant 100.0V input, while in the second set the voltage is varied along the length of the actuator. The results for both of these conditions are described next.

5.1. Constant Voltage


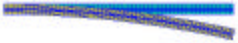
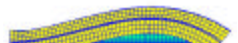

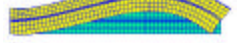
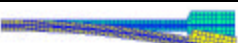
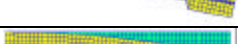

Optimization using both the response surface and kriging models yields results which agree with solutions obtained for a uniformly thick bimorph actuator, i.e., a thin bimorph results in large tip deflection, and a thick bimorph results in a large blocked force at the tip. The results of the optimization are shown in Table 3 for the maximum deflection and blocked force objectives subject to the constant voltage condition. However, since both tip deflection and force are to be maximized simultaneously, and these are conflicting design requirements, a multi-criteria type problem formulation is required to find a

compromise solution. Two multicriteria objectives were developed to simultaneously maximize the force and deflection performance of the bimorph. The first approach is to maximize the work produced at the tip of the bimorph, which is modeled as the product of the free displacement and blocked force and is measured in N-mm. Since maximum blocked force and maximum free deflection are not simultaneously achievable, this work term is a theoretical maximum; the actual work available is necessarily less than the product of the free deflection and the blocked force. The maximum work solution for the constant voltage condition is shown in Table 3, which is a compromise solution between the maximum deflection and maximum blocked force solutions.

An alternative multicriteria objective is the normalized weighted sum of the deflection and blocked force. Equation 10 describes this objective function, where w is a scalar weighting coefficient which can be selected by the designer to place more weight on one of the individual objectives. The d_{free}^* and $F_{blocked}^*$ are the individual optimum values of free deflection and blocked force, respectively. This objective function represents the distance from the utopia point⁴², which is the theoretical best performance point. This distance is minimized in order to produce a solution with the highest possible free deflection and blocked force.

$$f = (1 - w) \frac{d_{free}^* - d_{free}}{d_{free}^*} + (w) \frac{F_{blocked}^* - F_{blocked}}{F_{blocked}^*} \quad (10)$$

Table 3. Optimization Results.

Voltage Condition	Objective Function	Objective Function Value	t ₁	t ₂	t ₃	t ₄	t ₅	Percent Improvement w/Saturation	Solution
Constant	Maximum Deflection (mm)	0.0318	1.0	1.0	1.0	1.0	1.0	99.7	
Saturation	Maximum Deflection (mm)	0.0635	1.0	1.0	1.0	1.0	1.0		
Constant	Maximum Force (N)	0.4321	3.0	3.0	3.0	3.0	3.0	505.3	
Saturation	Maximum Force (N)	2.6155	3.0	3.0	3.0	3.0	3.0		
Constant	Maximum Work (N*mm)	0.0056	1.0	1.0	1.0	1.0	3.0	1273.2	
Saturation	Maximum Work (N*mm)	0.0769	3.0	3.0	3.0	3.0	3.0		
Constant	Minimum Weighted Sum	0.2488	1.0	1.0	1.0	1.0	1.0	9.5	
Saturation	Minimum Weighted Sum	0.2724	3.0	3.0	3.0	3.0	3.0		

A study is conducted to determine the effect of the value of the weighting factor w on the optimal solution in the weighted sum problem. The weighting factor is varied from 0.0 to 1.0, using increments of 0.01. Although we expect to obtain several intermediate solutions by varying the weighting factor, only the two extreme solutions and one intermediate solution are obtained using the response surface model. As the weight on the deflection is increased the maximum deflection solution is obtained until the weighting factor reaches 0.59, after which an intermediate solution is obtained until $w = 0.88$. The maximum force solution is obtained when the weighting factor is in the 0.89-1.00 range. Using the kriging model, three intermediate solutions are found by varying the starting point in the adaptive linear program algorithm. Tables 4 and 5 show the effect of the weighting factor on the optimal solutions when using the approximation models.

Table 4. Effect of Weighting Factor: Response Surface Model.

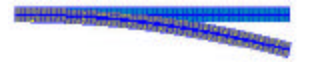
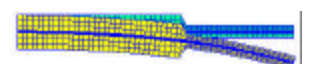
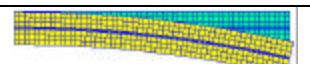
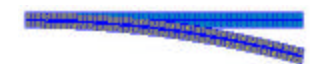
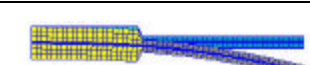
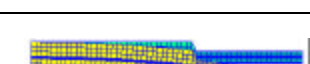


Weighting Factor, w	Optimal Solution	Predicted		ABAQUS	
		d (mm)	F_{blocked} (N)	d (mm)	F_{blocked} (N)
0.00 - 0.59		0.0318	0.2171	0.0317	0.1808
0.60 - 0.88		0.0096	0.4245	0.0092	0.4180
0.89 - 1.00		0.0052	0.4321	0.0048	0.4286

Table 5. Effect of Weighting Factor: Kriging Model

Weighting Factor, w	Optimal Solution	Predicted		ABAQUS	
		d (mm)	F_{blocked} (N)	d (mm)	F_{blocked} (N)
0.0-0.78		0.0317	0.1837	0.0317	0.1808
0.79		0.0143	0.2990	0.0148	0.3060
0.80-0.92		0.0092	0.4180	0.0092	0.4180
0.93-0.95		0.0082	0.4308	0.0082	0.3950
0.95-1.0		0.0048	0.4286	0.0048	0.4286

One advantage of using approximation methods such as response surfaces and kriging models is that the design space can be explored easily and rapidly. To further understand the tradeoff between the deflection and blocked force objectives, the metamodels are used to search the entire design space and identify the Pareto frontier. The design space is explored by predicting the response of 3125 design points using the kriging model. The Pareto frontier is obtained by selecting the points on the boundary of the design space as predicted by both the response surface and kriging models, as shown in Figure 7. A small subset of these points correspond to the solutions found by varying the weighting factor; however, rather than performing optimization with many values of weighting factors, Figure 7 illustrates that the Pareto frontier can be readily and easily captured using the metamodels themselves.

The Pareto design points, as predicted by the response surface and kriging models, are compared to one another and the points that have common thickness settings between the two are evaluated in ABAQUS to verify their actual response. The results of this analysis are also shown in Figure 7. One can see that the kriging model is a good predictor of the points along with Pareto frontier, while the response surface model is not as good a predictor of the response of points which have a large deflection and small blocked force. This result is consistent with the earlier finding that the response surface model is generally less accurate than the kriging model in predicting the response of a random set of points. It is also evident from

Figure 6 that by varying the thickness of the PZT layers a substantial blocked force can be generated, but the value of the tip deflection is still quite low when compared to the design requirements outlined in Table 1.

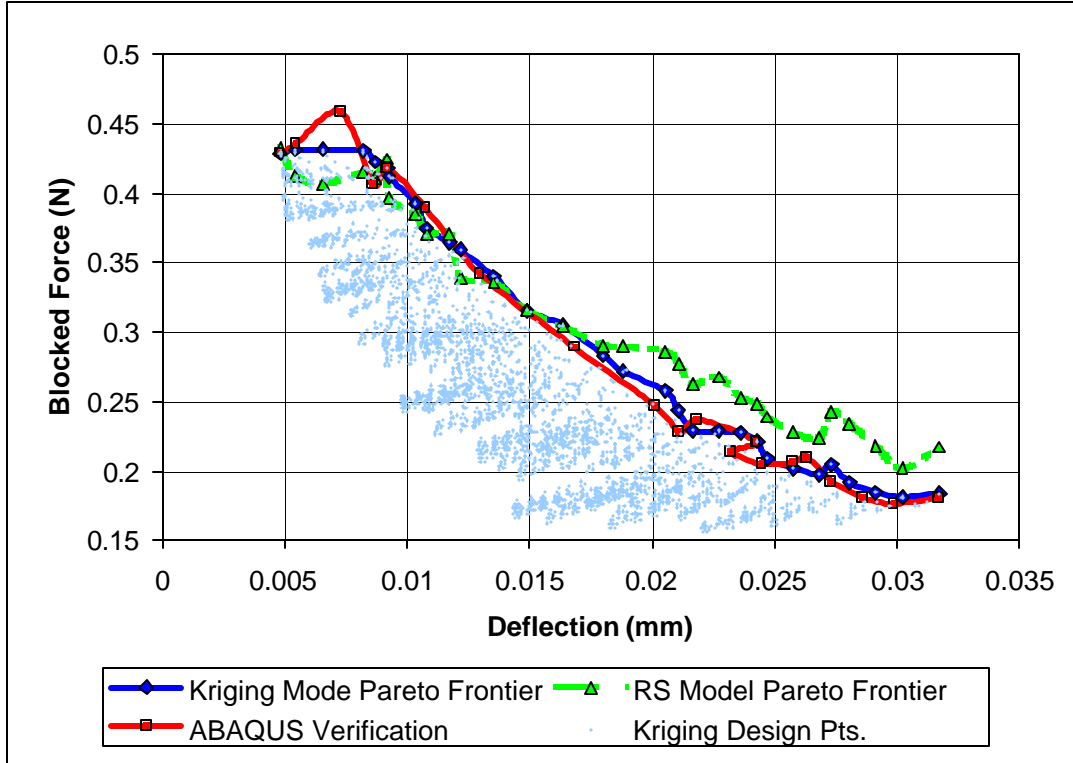


Figure 7. Design Space and Pareto Frontier – Constant Voltage.

5.2. Saturation Voltage

Further gains in deflection and blocked force performance can be obtained by varying the voltage applied to the PZT layers in addition to varying the thicknesses along the length of the bimorph. This phenomenon is explained by considering the electro-mechanical behavior of piezoceramic materials. Equation 11 represents the free strain produced in bending, where e is the free strain, d_{31} is the dielectric coefficient, V is the applied voltage, and t_c is the thickness of the PZT layer.

$$e = \frac{d_{31}V}{t_c} \quad (11)$$

As the previous optimization results indicate, a reduction in the piezoceramic layer thickness increases the free strain, resulting in an increased tip displacement. This process is limited by the saturation electric field, E_{sat} , which is a property of the particular piezoelectric material. The maximum voltage or saturation voltage, V_{sat} , which can be applied is limited by the thickness and the saturation electric field of a given material, as defined in Equation 12. By increasing the voltage applied to each PZT segment to its saturation voltage, the maximum induced strain can be obtained.

$$V_{sat} = E_{sat}t_c \quad (12)$$

Our analysis demonstrates that varying the voltage along the length of the bimorph actuator with each segment operating at its saturation voltage results in dramatic improvements in the tip deflection and force compared to the same bimorph with a constant applied voltage. The optimization process is repeated using both the response surface and kriging models, with each of the piezoceramic segments operating at its saturation voltage. The same solutions are obtained using both response

surfaces and kriging models for each objective function. The optimization results are previously summarized in Table 3, with $w = 0.5$ in the weighted sum objective. Note that while the same solution is found for the constant voltage and saturation voltage case for both maximum deflection and maximum blocked force, different solutions are obtained for the work and weighted sum objective functions. The maximum work and minimum weighted sum saturation voltage solutions are the same as the blocked force solution, indicating that the blocked force response dominates when using saturation voltages. In these two cases, the performance is improved more by increasing the applied voltage and therefore the section thicknesses than by just decreasing the piezoelectric layer thicknesses alone. With the thicker PZT layers, higher voltages are possible than with the thinner layers, allowing for more induced strain and therefore deflection and blocked force. In all cases, a dramatic improvement is achieved using saturation voltages compared to the constant voltage simulations.

The responses of the optimal solutions have been validated using ABAQUS. A comparison of these results is given in Table 6. Notice that the kriging model is a better predictor of the responses at the predicted optimal solution.

Table 6. Validation of Optimal Designs.

Voltage Condition	Objective Function	ABAQUS	RSM Predicted	RSM % Error	Kriging Predicted	Kriging % Error
Constant	Maximum Deflection (mm)	0.0317	0.0318	0.32	0.0317	0.00
Saturation	Maximum Deflection (mm)	0.0635	0.0635	0.00	0.0635	0.00
Constant	Maximum Force (N)	0.4286	0.4321	0.82	0.4286	0.00
Saturation	Maximum Force (N)	2.5722	2.6155	1.68	2.5722	0.00
Constant	Maximum Work (N*mm)	0.0054	0.0056	3.35	0.0054	0.00
Saturation	Maximum Work (N*mm)	0.0743	0.0769	3.45	0.0744	0.13
Constant	Minimum Weighted Sum	0.2891	0.2488	13.93	0.2855	1.25
Saturation	Minimum Weighted Sum	0.2748	0.2724	0.87	0.2723	0.55

When varying the value of the weighting the factor w in the weighted sum formulation, Equation 10, no intermediate points on the Pareto frontier are found when using the response surface model. Several intermediate solutions on the Pareto frontier are captured using the kriging model, but they are not evenly distributed across the frontier. Consequently, the new design space is searched by evaluating 3125 design points using the response surface and kriging models as shown in Figure 7, and the approximate Pareto frontier is selected from each set of points. The points that are common to both of these approximate Pareto frontiers are then evaluated in ABAQUS. Figure 8 illustrates that the kriging model is a good predictor of the response of these points, while the response surface model is a poor predictor of the response of the points with large deflection.

It is evident from Figure 8 that the Pareto frontier is not concave, indicating that a unique maximum combination of force and deflection does not exist. A compromise solution with thickness setting parameters of 2.5 mm, 2.0 mm, 2.0 mm, 1.0 mm, and 1.0 mm is selected as shown in Figure 8. This solution provides sufficient force performance for the intended application. The response as predicted by the kriging model is $F_{blocked} = 1.21$ N and $d_{free} = 0.0411$ mm. These values compare well to the ABAQUS predicted values of 1.16 N and 0.0413 mm, respectively.

The performance of the compromise solution with variable PZT layer thicknesses is compared to a standard bimorph with constant PZT layer thicknesses in Table 7. The two designs have equivalent volume of 510.0 mm³, and both are operated at their saturation voltage(s). One can see that a 37.6% gain in the blocked force performance is obtained by using the compromise design with varying PZT layer thicknesses.

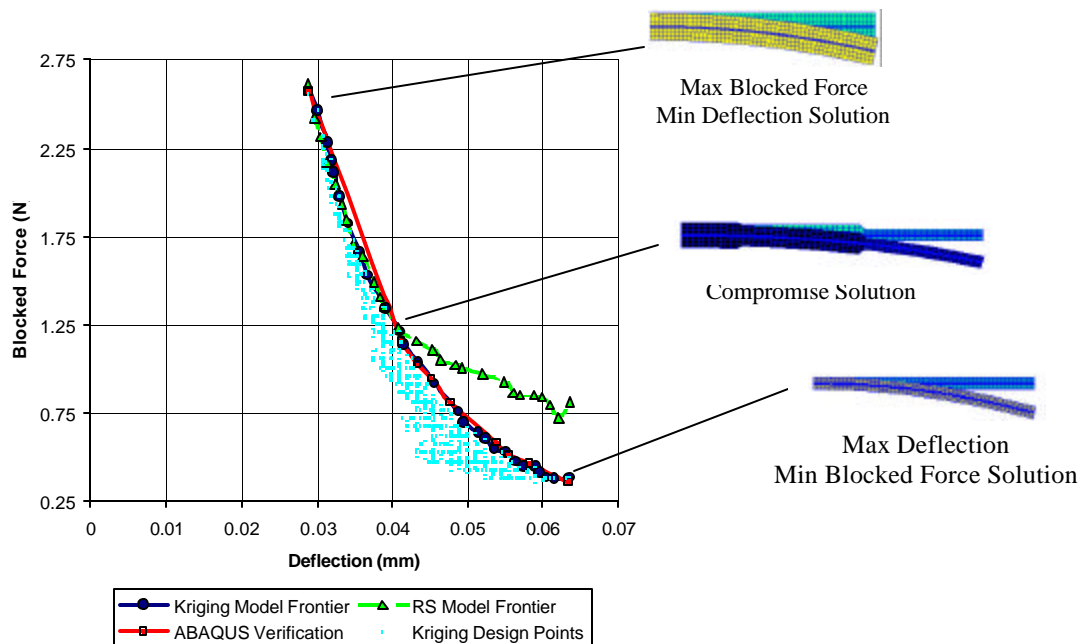


Figure 8. Design Space and Pareto Frontier – Saturation Voltage.

Table 7. Blocked Force Response of Compromise Solution and Straight Bimorph of Equivalent Volume.

		Objective Function Value	t ₁	t ₂	t ₃	t ₄	t ₅
Compromise Design	Maximum Force (N)	1.21	2.5	2.0	2.0	1.0	1.0
Constant Thickness Design	Maximum Force (N)	0.879	1.7	1.7	1.7	1.7	1.7

6. CONCLUSIONS

The tip deflection and force performance of a PZT bimorph actuator is improved by optimizing the thickness of the PZT layers when they are subject to a constant applied voltage. Dramatic improvements in performance are obtained by operating each PZT segment at its saturation voltage. To determine a compromise solution between the conflicting design objectives of maximum deflection and maximum force, two multicriteria objective functions are proposed: the product of the two objectives or work, and a weighted sum of the normalized objective functions. Multicriteria optimization using the metamodels tends to converge to either the lower or upper bound solutions, with very few intermediate solutions captured by varying the weighting factor. The metamodels prove to be a useful tool for quickly and efficiently visualizing the relationship between the competing objectives of force and deflection and are used to explore the design space rapidly to approximate the Pareto frontier. The kriging model is shown to be a more accurate predictor of the responses, particularly for the designs with high deflection and low force.

Ongoing work includes the testing of a scaled compromise solution prototype selected from the Pareto frontier. The experimental data will be used to validate the ABAQUS finite element model further along with the response surface and kriging models. A compromise solution produces sufficient force, but insufficient deflection according to the design requirements originally specified for the MIS application. Although significant improvements in performance are obtained by optimizing the thickness of the piezoceramic layers and varying the voltage applied to the layers, additional improvements in tip deflection are required for the MIS grasper application. Future work includes a feasibility study of alternative actuator materials with larger field induced strain such as piezoelectric polymers.

ACKNOWLEDGEMENTS

The support of the Charles E. Culpeper Foundation Biomedical Pilot Initiative is gratefully acknowledged by the first two authors. Support from ONR Contract # N00039-97-D-0042 is also acknowledged by the third author.

REFERENCES

1. Fatikow, S., and Rembold, U. (1997). *Microsystem Technology and Microrobotics*, Springer-Verlag Berlin Heidelberg.
2. Chonan, S., Jiang, Z. W., and Koseki, M. (1996). Soft-handling Gripper Driven by Piezoceramic Bimorph Strips. *Smart Mater. Struct.* 5, 407-414.
3. Seki, H. (1992). Piezoelectric Bimorph Microgripper Capable of Force Sensing and Compliance Adjustment. *Japan/USA Symposium on Flexible Automation. ASME 1992*, 1, 707-713.
4. Bar-Cohen, Y., Leary, S., Shahinpoor, M., Harrison, J. O., and Smith, J. (1999). Flexible Low-Mass Devices and Mechanisms Actuated by Electro-Active Polymers. *Proceedings SPIE Smart Structures and Materials*, Vol. 3669, pp. 51-56.
5. Lumia, R., and Shahinpoor, M. (1999). Microgripper Using Electro-Active Polymers. *Proceedings SPIE Smart Structures and Materials*, Vol. 3669, pp. 322-329.
6. Soper, N. J., Brunt, L. M., and Kerbl, K. (1994a). Laparoscopic General Surgery. *New England Journal of Medicine*, Feb. 10, 1994, Vol. 330, No. 6, pp. 409-419.
7. Soper, N. J., Odem, R. R., Clayman, R. V., and McDougall, E. M. (editors) (1994b). *Essentials of Laparoscopy*, Quality Medical Publishing, Inc., St. Louis.
8. Cohn, M., Crawford, L., Wendlandt, J., and Sastry, S. (1995). Surgical Applications of Milli-Robots. *Journal of Robotic Systems*, 12 (6), 401-416.
9. Hill, J., and Jensen, J. (1998). Telepresence Technology in Medicine: Principles and Applications. *Proceedings of the IEEE*, Vol. 86, No. 3, March, 1998, pp. 569-580.
10. Melzer, A. (1996). Endoscopic Instruments - Conventional and Intelligent. *Endosurgery*, Churchill Livingstone, New York, pp. 69-95.
11. Sastry, S., Cohn, M., and Tendick, F. (1997). Millirobotics for Remote Minimally Invasive Surgery. *Robotics and Autonomous Systems*, 21, 305-316.
12. Balazs, M., Feussner, H., Hirzinger, G., Omote, K., and Ungeheuer, A. (1998). A New Tool for Minor Access Surgery. *IEEE Engineering in Medicine and Biology*, May/June, 45-48.
13. Nakamura, Y., Matsui, A., and Saito, T. (1995). Shape Memory Alloy Active Forceps for Laparoscopic Surgery. *Proceedings of the IEEE International Conference on Robotics and Automation*.
14. Canfield, S., Edinger, B., Frecker, M., and Koopmann, G. (1999). Design of Piezoelectric Inchworm Actuator and Compliant End Effector for Minimally Invasive Surgery. *Proceedings SPIE 6th International Symposium on Smart Materials and Structures. Newport Beach, California, March, 1999*, Paper 3668-78.
15. ABAQUS Version 5.7-1 (1997). Hibbitt, Karlsson and Sorensen, Inc., 1080 Main Street, Pawtucket, Rhode Island 02860.
16. Mason, W. P., and Thurston, R. N. (1960). A Compact Electromechanical Band-Pass Filter for Frequencies Below 30 Kilocycles. *IRE Transactions on Ultrasonics Engineering*, June, 59-70.
17. Baz, A., and Poh, S. (1988). Performance of an Active Control System with Piezoelectric Actuators. *Journal of Sound and Vibration*, 126 (2), 327-343.
18. Cunningham, M. J., Jenkins, D. F. L., Clegg, W. W., and Bakush, M. M. (1995). Active Vibration Control and Actuation of a Small Cantilever for Applications in Scanning Probe Instruments. *Sensors and Actuators A* 50, 147-150.
19. Jenkins, D. F. L., Cunningham, M. J., and Clegg, W. W. (1995). The use of Composite Piezoelectric Thick Films for Actuation and Control of Miniature Cantilevers. *Microelectronic Engineering* 29, 71-74.
20. Kim, S. J. and J. D. Jones, (1991). Optimal Design of Piezoactuators for Active Noise and Vibration Control. *AIAA Journal* 29 (12) 2047-2053.
21. Crawley, E. F. and de Luis, J. (1987). Use of Piezoelectric Actuators as Elements of Intelligent Structures. *AIAA Journal* 25 (10), 1373-1385.

22. Cunningham, M. J., Jenkins, D. F. L., and Bakush, M. M. (1997). Experimental Investigation of Optimal Thickness of a Piezoelectric Element for Cantilever Actuation. *IEEE Proc-Sci. Meas. Technol.* 144 (1), 45-48.
23. Franco-Correia, V., Mota Soares, C. M., and Mota Soares, C. A. (1998). Modeling and Design of Adaptive Composite Structures. *Proceedings NATO Advanced Study Institute on Mechanics of Composite Materials and Structures, Troia, Portugal, Vol. II*, 59-92.
24. Low, T. S. and Guo, W. (1995). Modeling of a Three-Layer Piezoelectric Bimorph Beam with Hysteresis. *Journal of Microelectromechanical Systems.* 4 (4), 230-237.
25. Crawley, E. F. and Anderson, E. H. (1990). Detailed Models of Piezoceramic Actuation of Beams. *J. of Intell. Mater. Syst. and Struct.* 1, January, 4-25.
26. Wolf, K., Frese, S., Hagedorn, P., and Seemann, W. (1997) Thickness-Optimization of Piezoceramic Transducers for Energy Transfer. *Proceedings of the DETC'97, 1997 ASME Design Engineering Technical Conferences, Sacramento, California, September 14-17, 1997.* DETC97/VIB-3839.
27. Silva, E., Fonseca, J., Kikuchi, N. (1997). Optimal Design of Piezoelectric Microstructures. *Computational Mechanics*, 19, 397-410.
28. Montgomery, D. C. (1997). *Design and Analysis of Experiments*, Fourth Edition, John Wiley & Sons, New York.
29. Myers, R. H. and Montgomery, D. C. (1995). *Response Surface Methodology: Process and Product Optimization Using Designed Experiments*, John Wiley & Sons, New York.
30. MATLAB Version 5.1.0 (1997). The Math Works Inc., 24 Prime Park Way, Natick, MA 01760-1500.
31. Barton, R. R. (1992). Metamodels for Simulation Input-Output Relations. *Proceedings of the 1992 Winter Simulation Conference (Swain, J. J., Goldsman, D., et al., eds.)*, Arlington, VA, IEEE, pp. 289-299.
32. Toropov, V., van Keulen, F., Markine, V. and de Doer, H. (1996). Refinements in the Multi-Point Approximation Method to Reduce the Effects of Noisy Structural Responses. *6th AIAA/USAF/NASA/ISSMO Symposium on Multidisciplinary Analysis and Optimization*, Bellevue, WA, AIAA, Vol. 2, pp. 941-951. AIAA-96-4087-CP.
33. Rodriguez, J. F., Renaud, J. E. and Watson, L. T. (1997). Trust Region Augmented Lagrangian Methods for Sequential Response Surface Approximation and Optimization. *Advances in Design Automation (Dutta, D., ed.)*, Sacramento, CA, ASME, Paper No. DETC97/DAC-3773.
34. Koch, P. N., Simpson, T. W., Allen, J. K. and Mistree, F. (1999). Statistical Approximations for Multidisciplinary Optimization: The Problem of Size. *Special Multidisciplinary Design Optimization Issue of Journal of Aircraft*, Vol. 36, No. 1, pp. 275-286.
35. Cressie, N. A. C. (1993). *Statistics for Spatial Data*. New York, John Wiley & Sons.
36. Simpson, T. W., Peplinski, J., Koch, P. N., and Allen, J. K. (1997). On the Use of Statistics in Design and the Implications for Deterministic Computer Experiments. *Proceedings of the DETC'97, 1997 ASME Design Engineering Technical Conferences, Sacramento, California, September 14-17, 1997.* DETC97/DTM-3881.
37. Sacks, J., Welch, W. J., Mitchell, T. J. and Wynn, H. P. (1989). Design and Analysis of Computer Experiments. *Statistical Science*, Vol. 4, No. 4, pp. 409-435.
38. Simpson, T. W., Allen, J. K. and Mistree, F. (1998). Spatial Correlation Metamodels for Global Approximation in Structural Design Optimization. *Advances in Design Automation*, Atlanta, GA, ASME, Paper No. DETC98/DAC-5613.
39. Goffe, W. L., et al. (1994). "Global Optimization of Statistical Functions with Simulated Annealing." *Journal of Econometrics* 60(1-2), 65-100. Source code is available online at <http://netlib2.cs.utk.edu/opt/simann.f>.
40. Mistree, F., Hughes, O. F. and Bras, B. A. (1993). The Compromise Decision Support Problem and the Adaptive Linear Programming Algorithm. *Structural Optimization: Status and Promise (Kamat, M. P., ed.)*, AIAA, Washington, D.C., pp. 247-289.
41. McKay, M. D., Beckman, R. J. and Conover, W. J. (1979). A Comparison of Three Methods for Selecting Values of Input Variables in the Analysis of Output from a Computer Code. *Technometrics*, 21 (2), 239-245.
42. Stadler, W., ed. (1988). *Multicriteria Optimization in Engineering and in the Sciences*, Pelnum Press, New York.

APPENDIX

Finite Element Model Parameters for 54.0 mm Long Segmented Bimorph.

Piezoelectric layer material: PZT5H	Middle Beam Material: Steel
Middle Beam Thickness=0.5mm	Input Voltage=100.0 V
High PZT Thickness=3.0 mm	Section Length=10.0 mm
Medium PZT Thickness=2.0 mm	Transition Element Length=1.0 mm
Low PZT Thickness=1.0 mm	Width=3.0 mm

Material Properties for PZT5H:

Density=7500.0 kg/m³

Piezoelectric Strain Matrix:

$$S = \begin{bmatrix} 0 & -274 & 0 \\ 0 & 500.6 & 0 \\ 0 & -274 & 0 \\ 741 & 0 & 0 \\ 0 & 0 & 0 \\ 0 & 0 & 495.71 \end{bmatrix} \frac{m}{V}$$

Elasticity Matrix:

$$E = \begin{bmatrix} 126 & 7.95 & 8.41 & 0 & 0 & 0 \\ 7.95 & 126 & 8.41 & 0 & 0 & 0 \\ 8.41 & 8.41 & 11.7 & 0 & 0 & 0 \\ 0 & 0 & 0 & 2.33 & 0 & 0 \\ 0 & 0 & 0 & 0 & 2.3 & 0 \\ 0 & 0 & 0 & 0 & 0 & 2.3 \end{bmatrix} \times 10^{10} \frac{N}{m^2}$$

Dielectric Matrix:

$$D = \begin{bmatrix} 1.503 & 0 & 0 \\ 0 & 1.503 & 0 \\ 0 & 0 & 1.3 \end{bmatrix} \times 10^{-9} \frac{F}{m}$$

Material Properties for Steel:

Density=7850.0 kg/m³

Modulus of Elasticity=20.0 GPa

$\nu = 0.30$